International Journal of Mechanical Sciences 53 (2011) 338–347

Contents lists available at ScienceDirect

International Journal of Mechanical Sciences

journal homepage: www.elsevier.com/locate/ijmecsci

Prediction of anisotropy and hardening for metallic sheets in tension, simple shear and biaxial tension

S.L. Zang [a,b,1], S. Thuillier [a,b,*], A. Le Port [a,b], P.Y. Manach [a,b]

[a] LIMATB, Université de Bretagne-Sud, Rue de Saint Maudé, BP 92116, F-56321 Lorient, France
[b] Université européenne de Bretagne, France

ARTICLE INFO

Article history:
Received 15 May 2010
Received in revised form
4 November 2010
Accepted 9 February 2011
Available online 21 February 2011

Keywords:
Anisotropic yield
Constitutive behavior
Metallic material
Mechanical testing

ABSTRACT

The mechanical behavior of mild and dual phase steel sheets is investigated at room temperature in quasi-static conditions under different strain paths: uniaxial tension, simple shear and balanced biaxial tension. The aim is to characterize both the anisotropy and the hardening, in order to identify material parameters of constitutive equations able to reproduce the mechanical behavior. In particular, a good description of flow stress levels in tension and shear as well as plastic anisotropy coefficients is expected. Moreover, the Bauschinger effect is investigated with loading–reloading in the reverse direction shear tests and the balanced biaxial tension test gives insight of the mechanical behavior up to very high equivalent plastic strains. Yoshida–Uemori hardening model associated with Bron–Besson orthotropic yield criterion is used to represent the in-plane mechanical behavior of the two steels. The identification procedure is based on minimization of a cost function defined over the whole database. The presented results show a very good agreement between model predictions and experiments: flow stress during loading and reverse loading as well as plastic anisotropy coefficients are well reproduced; it is shown that the work-hardening stagnation after strain path reversal is well estimated in length but Yoshida–Uemori model underestimates the rate of work-hardening.

1. Introduction

Nowadays, phenomenological models are widely used in finite element analysis of sheet metal forming process, since they present a good compromise between simulation accuracy and computation time. Such models of the elasto-viscoplastic behavior of sheet metals are based on the definition of a yield surface, to describe the initial anisotropy related to the crystallographic texture, and its evolution with plastic strain. Initial orthotropy is a good representation for rolled sheets and is assumed to be kept during strain, by considering a corotation of the anisotropy frame with material rotation. Strain-induced anisotropy, such as Bauschinger effect, is described by the evolution of internal variables with plastic strain. Several experimental tests, like tension-compression [1,2] and simple shear [3], have been performed to characterize the hardening behavior of sheet metals under strain reversal, which refers to the fact that the subsequent loading direction is opposite to that of former loading, and is quite common in sheet metal forming processes; for example, bending–unbending on the die radius and reverse bending–unbending at the punch nose. This behavior under strain reversal, called the Bauschinger effect, is characterized by a lower yield stress under strain reversal, further transient behavior that corresponds to the smooth elastic-plastic transition with a rapid change of strain-hardening rate, and a hardening stagnation, the magnitude of which depends on the prestrain and permanent softening characterized by stress offset.

The prediction of the anisotropy and hardening of metallic sheets depends not only on the constitutive model but also on the accurate material parameter identification which refers both to the type of the experimental tests being used and the identification methods. Tension, simple shear and balanced biaxial tension tests provide relevant information on the shape of the yield surface and its evolution with plastic strain. However, current researches seldom consider all of them to identify the material parameters. The general identification strategy is that the first step is the identification of the initial yield surface, using either the yield stresses or the anisotropy coefficients, or both, and the second step is the hardening behavior, e.g. [4].

In the present study, an alternative procedure is used and the material parameters of both the yield function and the hardening model are identified from the stress–strain curves and both longitudinal and transverse strain in tension at the same time. The constitutive equations are derived from Bron–Besson yield

* Corresponding author at: LIMATB, Université de Bretagne-Sud, Rue de Saint Maudé, BP 92116, F-56321 Lorient, France. Tel.: +33 297874570; fax: +33 297874572.
E-mail address: sandrine.thuillier@univ-ubs.fr (S. Thuillier).
[1] Present address: School of Mechanical Engineering, Xi'an Jiaotong University, No. 28, Xianning Road, Xi'an, Shaanxi, China.

0020-7403/$ - see front matter © 2011 Elsevier Ltd. All rights reserved.
doi:10.1016/j.ijmecsci.2011.02.003

function [5] and Yoshida–Uemori hardening model [6] and identification of material parameters in tension, monotonic and Bauschinger simple shear and balanced biaxial tension tests are presented for DP500 and DC04 steels: balanced biaxial tension allows to reach high equivalent plastic strain, whereas simple shear involves large material rotations. Considering these three tests leads to a complementary experimental database well suited for phenomenological approach, though it is rather constraining for parameter identification. The ability of Yoshida–Uemori model to predict the work-hardening stagnation after strain path reversal in simple shear is particularly studied. This test allows an equivalent plastic prestrain up to 0.2 to be investigated and to reach after straining an equivalent plastic strain of 0.5.

2. Experiments

Two thin sheet materials are considered in this study: a mild steel DC04, with a thickness $e = 0.67$ mm and a dual phase steel with a thickness of 0.6 mm and a tensile strength of 500 MPa (DP500). For this last material, SEM micrographs have evidenced a volume fraction of martensite around 6% and a grain size of 5 μm. The mechanical behavior of these two steels is investigated under three different stress and strain states, i.e. uniaxial tension, simple shear (both of these tests are performed at several orientations to the rolling direction or RD) and balanced biaxial tension. The experimental procedure is described in the following paragraphs.

2.1. Tension

Tensile tests were carried out on rectangular samples of dimension 20 $\times$180 $\times$e mm^3. The free edges were machined in order to eliminate the hardened areas induced by the cutting and thus to increase the range of homogeneous deformation. Components of the strain tensor in the sheet plane are calculated by image correlation. Monotonous tensile tests were carried out at 0°, 45° and 90° to the RD for DP500 and in addition at 22° and 77° for DC04, in order to study the material anisotropy. For these tests, a cross-head speed of 10 mm/min is imposed which leads to $\dot{\varepsilon} \simeq 2.4 \times 10^{-3}$ s^{-1}. The logarithmic strain as well as the Cauchy stress are calculated from the raw data (Fig. 1). The plastic anisotropy coefficients $r_\alpha = d\varepsilon^p_{YY}/d\varepsilon^p_{ZZ}$, where $\vec{e}_X$ denotes the tensile, $\vec{e}_Y$ the transverse and $\vec{e}_Z$ the normal directions, respectively, and α the angle between the RD and the tensile direction, are calculated from the transverse strain ε_{YY} and the assumption of volume conservation in the plastic area; they are given in Table 1.

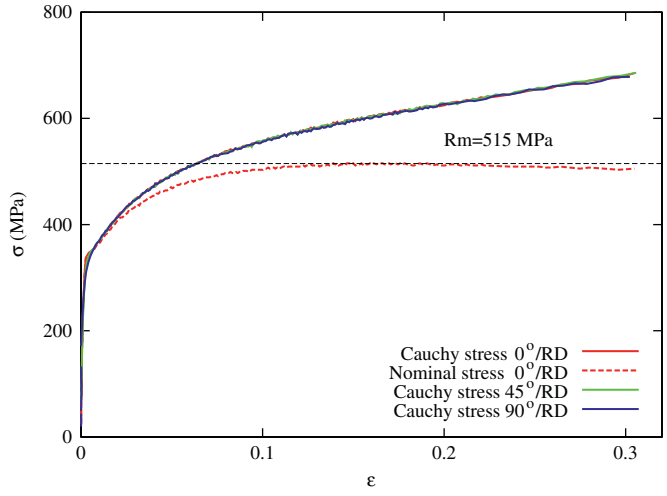

Fig. 1. Cauchy stress versus logarithmic longitudinal strain evolution for DP500 in tension. The strain range is investigated a little further necking, evidenced on the nominal stress–strain curve, and by neglecting any triaxiality effects in this area. This assumption has been validated by finite element simulation.

The deformation gradient $\boldsymbol{F}$ [7] in the central zone of the sample is given by $\boldsymbol{F} = F_{XX}\vec{e}_X \otimes \vec{e}_X + F_{YY}\vec{e}_Y \otimes \vec{e}_Y + F_{ZZ}\vec{e}_Z \otimes \vec{e}_Z$ where $\vec{e}_i, i = X,Y,Z$ are the basis vectors of the global reference frame. The test is controlled by the evolution of F_{XX} with time and by constraining $\sigma_{YY} = \sigma_{ZZ} = 0$. The signals calculated from the recorded raw data are the components F_{YY} and σ_{XX} = load/(actual section). The strain range is limited to its maximum value before necking, which corresponds to 0.18 for DP500 and 0.25 for DCO4, whatever the orientation to RD.

2.2. Simple shear

The simple shear device is presented in detail in [8]. The specimens have a rectangular shape, a gauge area of length L = 50 mm and width h of 4 mm; the shear direction is along the length of the specimen (Fig. 2). The samples are kept under the grips by six screws tightened by a dynamometric key which torque is calibrated depending on the tested material. The optimal value is obtained with the lowest torque that minimizes the sliding between the sample and the grips. Monotonous shear tests were performed on samples at the same orientations to the RD than for the tensile test, at a cross-head speed of 0.5 mm/min, which corresponds to $\dot{\gamma} = 2.1 \times 10^{-3}$ s^{-1}. Moreover, cyclic tests are performed in order to highlight the Bauschinger effect and to measure kinematic hardening parameters. These tests are composed of a loading up to several values of γ followed by a load in the opposite direction until $\gamma = -0.4$. Each kind of test is performed three times to check the reproducibility and a representative test is chosen for the database. Shear strain γ, which corresponds to the non-diagonal component of the planar transformation gradient in the case of an ideal simple shear kinematics [8], is measured from a digital correlation system and is then defined as an average over a rectangular zone on the sample surface. Fig. 2 shows a rather constant value of γ except near the free ends of the specimen, over a distance of approximately 5 mm.

The kinematics of the simple shear test can be described by $\boldsymbol{F} = \boldsymbol{I} + F_{XY}\vec{e}_X \otimes \vec{e}_Y$ with $\boldsymbol{I}$ the second order identity tensor. The test is controlled by the evolution of F_{XY} with time, where $\vec{e}_X$ is parallel to the shear direction and $\vec{e}_Y$ perpendicular to $\vec{e}_X$ in the sheet plane, and by constraining $\sigma_{iZ} = 0 (i = X,Y,Z)$. This assumption of a planar stress state comes from the small sheet thickness.

2.3. Balanced biaxial tension

A hydraulic bulge test, developed in the Université de Bretagne-Sud (A. Penin, V. Grolleau, unpublished results, 2001),

Table 1
Plastic anisotropy coefficients of the two steels. The average anisotropy coefficient $\bar{r} = (r_0 + r_{90} + 2r_{45})/4$, which characterizes the normal anisotropy and the planar anisotropy, measured by the coefficient $\Delta r = (r_0 + r_{90} - 2r_{45})/2$ are also given.

Material	r_0	r_{22}	r_{45}	r_{77}	r_{90}	$\bar{r}$	Δr
DC04	1.680 ±0.025	1.680 ±0.0316	1.890 ±0.051	2.206 ±0.035	2.253 ±0.062	1.928	0.08
DP500	0.866 ±0.005	–	1.040 ±0.01	–	1.033 ±0.005	0.995	0.09

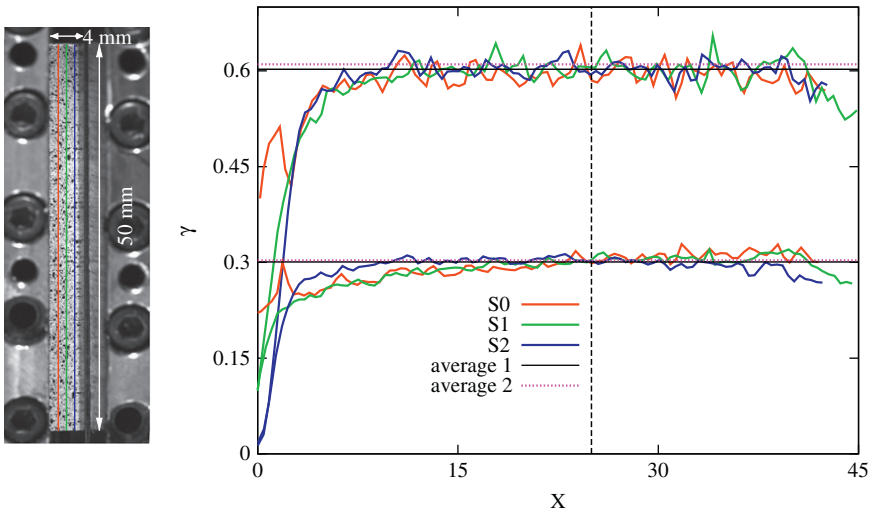

Fig. 2. Homogeneity of the strain distribution along three sections (S_0, S_1, S_2) parallel to the shear direction, for $\gamma = 0.3$ and 0.6. X is along the sample length. Either the entire gauge surface is used (average 1) or a reduced area in the specimen center (average 2). In the following, the second measure is used.

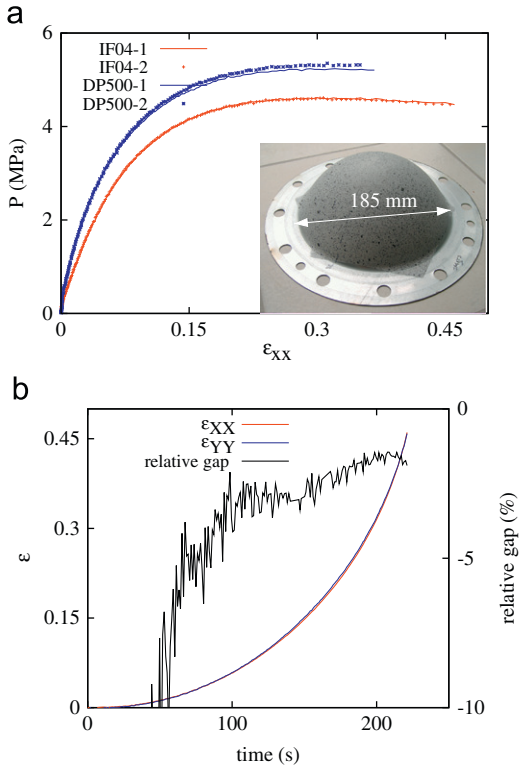

Fig. 3. Biaxial expansion. (a) Evolution of pressure P versus ε_{XX} in balanced biaxial expansion. Two tests for each material are plotted to show the good reproducibility obtained. (b) Comparison of ε_{XX} and ε_{YY} for material DC04. The relative gap is defined by $(\varepsilon_{XX}-\varepsilon_{YY})/\varepsilon_{XX}$.

is used to obtain a balanced biaxial strain state. Circular blanks of gauge diameter of 185 mm are clamped by screws between a blank-holder and a die with a radius of 8 mm. A fixed volume of water is pressed under the blank by the displacement of an actuator. A pressure sensor gives the fluid pressure and the strain field is measured by digital correlation in an area around the center point (Fig. 3(a)). The strain state on the surface is recorded during the test; an average of the strain components over a small area around the specimen center is performed and the evolution of ε_{XX} and ε_{YY} with time is compared (Fig. 3(b)), with $\vec{e}_X$ parallel to the RD and $\vec{e}_Y$ its perpendicular in the sheet plane. It can be shown that the two components are very close to each other for both materials, though only one (DC04) is presented here. The relative gap $(\varepsilon_{XX}-\varepsilon_{YY})/\varepsilon_{XX}$ is lower than 4%, for strains above 0.05. The curvature radius R_{BT} is determined by fitting a sphere over the selected area, which leads to an average value. A balanced biaxial stress state is assumed and its non-zero component is calculated from the bulging pressure P and the current blank thickness e:

$$\sigma_b = \frac{PR_{BT}}{2e} \tag{1}$$

As shown in Fig. 3(a), $\varepsilon_{XX} \approx \varepsilon_{YY}$ and, therefore, a balanced biaxial strain state is imposed. In the identification procedure, the bulge test is considered as a homogeneous test with $\boldsymbol{F} = F_{XX}(\vec{e}_X \otimes \vec{e}_X + \vec{e}_Y \otimes \vec{e}_Y) + F_{ZZ}\vec{e}_Z \otimes \vec{e}_Z$. The test is controlled by the evolution of F_{XX} with time, and the stress tensor is given by $\boldsymbol{\sigma} = \sigma_b(\vec{e}_X \otimes \vec{e}_X + \vec{e}_Y \otimes \vec{e}_Y)$. The strain range is limited to its maximum value before localization, evidenced by the pressure decrease, which corresponds to 0.3 for both DP500 and DCO4.

3. Constitutive equations

In this paper, the material model is a modification of the elasto-plastic model of [6] in which Bron–Besson non-quadratic orthotropic yield function [5], a non-saturating isotropic strain-hardening and the viscous character of the material are taken into account. Moreover, constitutive equations are written in the anisotropy frame {RD,TD,ND}, the orientation of which is constant during deformation compared to the corotational frame. After each increment, the tensorial variables are rotated back to the corotational frame and then to the global reference frame. In the following, the corotated strain tensor $\boldsymbol{\varepsilon}$, elastic strain $\boldsymbol{\varepsilon}^e$, viscoplastic strain $\boldsymbol{\varepsilon}^{vp}$ and Cauchy stress $\boldsymbol{s}$ in the anisotropy frame are used.

3.1. Hardening model

In elasto-viscoplastic constitutive model, the rate of $\boldsymbol{s}$ can be written as

$$\dot{\boldsymbol{s}} = \boldsymbol{C} : (\dot{\boldsymbol{\varepsilon}} - \dot{\boldsymbol{\varepsilon}}^{vp}) \tag{2}$$

where $\boldsymbol{C}$ is the elasticity modulus tensor.

The viscoplastic strain tensor follows a flow rule derived from a viscoplastic potential Ω which is a power function of overstress

$\boldsymbol{s}_v = f_+ > 0$ or viscous stress [9]:

$$\Omega(f) = \frac{K_v}{n_v+1}\left(\frac{f_+}{K_v}\right)^{n_v+1} \tag{3}$$

where n_v is the strain rate sensitivity coefficient and K_v a weighting coefficient of the viscous part of the stress. The behavior is thus elastic if $f \le 0$ and if $f > 0$, the viscoplastic strain rate is written as

$$\dot{\boldsymbol{\varepsilon}}^{vp} = \frac{\partial \Omega}{\partial \boldsymbol{s}} = \Omega'(f)\frac{\partial f}{\partial \boldsymbol{s}} \tag{4}$$

The equivalent viscoplastic strain rate $\dot{p}$ is defined by

$$\dot{p} = \sqrt{\frac{2}{3}\dot{\boldsymbol{\varepsilon}}^{vp} : \dot{\boldsymbol{\varepsilon}}^{vp}} \tag{5}$$

The model proposed by Yoshida and Uemori [6] is constructed within the framework of two-surface modeling [10]; only kinematic hardening of the yield surface f is assumed, but mixed isotropic-kinematic hardening for the bounding surface G:

$$f = \phi(\boldsymbol{s},\boldsymbol{\alpha}) - Y = 0 \tag{6}$$

where ϕ is a scalar function measuring the size of the yield surface, the second order tensor $\boldsymbol{\alpha}$ is a back-stress representing the center of the yield surface, and Y is fixed and represents the initial yield stress.

The bounding surface is described by the equation:

$$G = \phi(\boldsymbol{\Sigma},\boldsymbol{\beta}) - (B+R) = 0 \tag{7}$$

where $\boldsymbol{\Sigma}$ is a stress tensor, $\boldsymbol{\beta}$ denotes the center of the bounding surface, and B and R are, respectively, the initial size and the isotropic hardening (IH) component of the bounding surface.

The kinematic hardening of the yield surface is calculated from:

$$\boldsymbol{\alpha} = \boldsymbol{X} + \boldsymbol{\beta} \tag{8}$$

Evolution of back-stress tensor $\boldsymbol{X}$ is defined as

$$\dot{\boldsymbol{X}} = C\left[\left(\frac{a}{\overline{s}}\right)(\boldsymbol{s}-\boldsymbol{\alpha}) - \sqrt{\frac{a}{\overline{\boldsymbol{X}}}}\boldsymbol{X}\right]\dot{p} \quad \text{with} \quad \overline{\boldsymbol{X}} = \phi(\boldsymbol{X}) \quad \text{and} \quad a = B+R-Y \tag{9}$$

where C is a material parameter that controls the rate of the kinematic hardening.

The following evolution equation is assumed to describe the kinematic hardening of the bounding surface:

$$\dot{\boldsymbol{\beta}} = m\left(\frac{2}{3}b\dot{\boldsymbol{\varepsilon}}^{vp} - \boldsymbol{\beta}\dot{p}\right) \tag{10}$$

where m and b denote material parameters.

In the present paper, the Swift law is used to describe the non-saturating strain-hardening for some materials within certain range of large strain instead of Voce law [11]:

$$\dot{R} = nK(p+\varepsilon_0)^{n-1}\dot{p} \quad \text{with} \quad \varepsilon_0 = \left(\frac{B}{K}\right)^{1/n} \tag{11}$$

where K is a material parameter and n the hardening coefficient.

Hardening stagnation recorded after strain path reversal is modeled by the non-isotropic hardening (non-IH) of the bounding surface; a non-IH surface, g_s, is defined in the stress space:

$$g_s(\boldsymbol{s},\boldsymbol{q},r) = \psi(\boldsymbol{s}-\boldsymbol{q}) - r = \sqrt{\frac{3}{2}(\boldsymbol{s}-\boldsymbol{q}) : (\boldsymbol{s}-\boldsymbol{q})} - r = 0 \tag{12}$$

where $\boldsymbol{q}$ and r denote the center and size of the non-IH surface, respectively. The center of the bounding surface, $\boldsymbol{\beta}$, exists either on or inside the surface g_s. The isotropic hardening of the bounding surface takes place only when the center point of the bounding surface, $\boldsymbol{\beta}$, lies on the surface g_s, namely $\dot{R} > 0$ when

$$g_s(\boldsymbol{\beta},\boldsymbol{q},r) = 0 \tag{13a}$$

$$\frac{\partial g_s(\boldsymbol{\beta},\boldsymbol{q},r)}{\partial \boldsymbol{\beta}} : \dot{\boldsymbol{\beta}} > 0 \tag{13b}$$

otherwise

$$\dot{R} = 0 \tag{14}$$

A kinematic motion of the surface g_s such that the center of g_s moves in the direction of $(\boldsymbol{\beta}-\boldsymbol{q})$ is assumed:

$$\dot{\boldsymbol{q}} = \mu(\boldsymbol{\beta}-\boldsymbol{q}) \tag{15}$$

From the consistency condition that the center of the bounding surface, $\boldsymbol{\beta}$, should be either on or inside g_σ, this leads to

$$\mu = \frac{1}{\psi(\boldsymbol{\beta},\boldsymbol{q})}\left(\frac{\partial \psi(\boldsymbol{\beta},\boldsymbol{q})}{\partial \boldsymbol{\beta}} : \dot{\boldsymbol{\beta}} - \dot{r}\right) \tag{16}$$

The following evolution equation for r is assumed:

$$\dot{r} = h\Gamma, \quad \Gamma = \frac{\partial \psi(\boldsymbol{\beta},\boldsymbol{q})}{\partial \boldsymbol{\beta}} : \dot{\boldsymbol{\beta}} \quad \text{when} \quad \dot{R} > 0 \tag{17a}$$

$$\dot{r} = 0, \quad \text{when} \quad \dot{R} = 0 \tag{17b}$$

where $h (0 \le h \le 1)$ denotes a material parameter that determines the rate of expansion of the surface g_s. With the help of Eq. (17a), μ is rewritten by

$$\mu = \frac{1}{\psi(\boldsymbol{\beta},\boldsymbol{q})}(1-h)\Gamma \tag{18}$$

Since the non-IH (strain-hardening stagnation) appears during reverse deformation after prestrain, the initial value of r may be assumed to be zero, which is different with Yoshida's assumption of r with a very small initial value.

There are altogether eight material parameters to be identified when using Yoshida–Uemori hardening law: Y, B, C, m, b, h, K, and n. Moreover, out of comparison's sake, a power-law (Swift) hardening was also used and in this case, three parameters are identified: Y, K and n according to Eq. (11).

3.2. Hill's 1948 yield stress function

Hill's 1948 quadratic anisotropic yield function [12] can be written as

$$\phi(\boldsymbol{s}) = \overline{s} = \sqrt{F(s_{22}-s_{33})^2 + G(s_{33}-s_{11})^2 + H(s_{11}-s_{22})^2 + 2Ls_{23}^2 + 2Ms_{31}^2 + 2Ns_{12}^2} \tag{19}$$

where $\overline{s}$ is the equivalent stress, and 1, 2, 3 stand for the RD, TD and ND, respectively. F, G, H, L, M and N are material parameters.

The condition on the initial elastic limit along the RD imposes the relation $G+H=1$. In the case of sheet materials, mechanical tests involving σ_{i3} are rather difficult to perform and therefore, in the following, it is assumed that L and M are kept equal to their value in case of an isotropic behavior, i.e. $L=M=$ 1.5. There are then three material parameters to identify: F, G and N.

3.3. Bron–Besson yield stress function

The classically used form of [5] yield function is defined by an equivalent stress:

$$\phi(\boldsymbol{s}) = \overline{s} = \left(\sum_{k=1}^{2}\alpha^k(\overline{s}^k)^a\right)^{1/a} \tag{20}$$

where $\overline{s}^k$ are one order positive and homogeneous functions which are convex with respect to $\boldsymbol{s}$. α^k are the weights of each function $\overline{s}^k$ and positive coefficients, the sum of which is equal to 1. The functions are defined by

$$\overline{s}^k = (\psi^k)^{1/b^k} \tag{21}$$

where

$$\psi^1 = \tfrac{1}{2}\left(|S_2^1 - S_3^1|^{b^1} + |S_3^1 - S_1^1|^{b^1} + |S_1^1 - S_2^1|^{b^1}\right)$$

$$\psi^2 = \frac{3^{b^2}}{2^{b^2}+2}\left(|S_1^2|^{b^2} + |S_2^2|^{b^2} + |S_3^2|^{b^2}\right)$$

In Eq. (21), $S^k_{i=1,3}$ are the principal values of a modified stress deviator $\boldsymbol{s}^k$, whose components are obtained from the following linear transformation of the Cauchy stress $\boldsymbol{s}$, which can be represented by a six-component vector $(s_{11},s_{22},s_{33},s_{12},s_{23},s_{31})^T$:

$$\boldsymbol{s}^k = \boldsymbol{L}^k : \boldsymbol{s} \tag{22}$$

where

$$\boldsymbol{L}^k = \begin{pmatrix} (c_2^k + c_3^k)/3 & -c_3^k/3 & -c_2^k/3 & 0 & 0 & 0 \\ -c_3^k/3 & (c_3^k + c_1^k)/3 & -c_1^k/3 & 0 & 0 & 0 \\ -c_2^k/3 & -c_1^k/3 & (c_1^k + c_2^k)/3 & 0 & 0 & 0 \\ 0 & 0 & 0 & c_4^k & 0 & 0 \\ 0 & 0 & 0 & 0 & c_5^k & 0 \\ 0 & 0 & 0 & 0 & 0 & c_6^k \end{pmatrix} \tag{23}$$

The anisotropy of Bron–Besson yield function is represented by 12 parameters, $c^{k=1-2}_{i=1-6}$, in the form of two fourth order symmetric tensors $\boldsymbol{L}^1$, $\boldsymbol{L}^2$. The other parameters a, b^1, b^2 and $\alpha = \alpha^1$ ($\alpha^2 = 1-\alpha^1$) only influence the shape of the yield surface. Thereby, the yield function has a total of 16 parameters. Note that the convexity and derivability of the yield surface are well proven for $a \geq 1$ and $b^k \geq 2$.

As for Hill's 1948 yield criterion, parameters $c_5^{k=1-2}$ and $c_6^{k=1-2}$ which are related to shear in the sheet thickness are kept equal to 1. There are, therefore, 12 material parameters to identify: $c^{k=1-2}_{i=1-4}$, a, b^1, b^2 and α.

3.4. Large strain framework

These constitutive equations have been implemented within SiDoLo software, which is a tool box for model development based on differential equations and for material parameter identification. The general framework is elasto-visco-plasticity in finite strains, by the use of the corotational frame to fulfill the material frame indifference requirement. This frame is associated to the skew-symmetric part $\boldsymbol{W}$ of the velocity gradient $\boldsymbol{L}$. Let $\boldsymbol{Q}^c$ be the rotation between the current space frame and the corotational frame, $\dot{\boldsymbol{Q}}^c\,{}^t\boldsymbol{Q}^c = \boldsymbol{W}$. An additive decomposition of the strain rate tensor in the corotational frame is chosen:

$$\dot{\boldsymbol{e}} = (\boldsymbol{Q}^c)^T \boldsymbol{D} \boldsymbol{Q}^c = \dot{\boldsymbol{e}}^e + \dot{\boldsymbol{e}}^{in} \tag{24}$$

with the strain rate tensor $\boldsymbol{D} = \boldsymbol{L} - \boldsymbol{W}$. Constitutive laws are written in the corotational frame, using the corotated Cauchy stress tensor $\boldsymbol{s}$ defined by

$$\boldsymbol{s} = (\det \boldsymbol{F})(\boldsymbol{Q}^c)^T \boldsymbol{\sigma} \boldsymbol{Q}^c \tag{25}$$

with $\boldsymbol{F}$ the transformation gradient and $\boldsymbol{\sigma}$ the Cauchy stress tensor. The associated derivative is then the Jaumann derivative. Within the SiDoLo environment, homogeneous mechanical tests are reproduced by defining either components of the transformation gradient or the stress tensor.

4. Results and discussion

4.1. Parameter identification

Inverse identification of the material parameters is carried out by optimization using uniaxial tensile, simple shear and balanced biaxial tensile tests with the software SiDoLo [13]. The cost function $\mathcal{L}(\boldsymbol{A})$ is defined in the least square sense by Eq. (26) and is minimized with a Levenberg–Marquardt algorithm, starting from an initial guess of material parameters $\boldsymbol{A}_0$.

$$\begin{aligned}\mathcal{L}(\boldsymbol{A}) &= \sum_{n=1}^{N} \mathcal{L}_n(\boldsymbol{A}) \\ &= \sum_{\alpha} \mathcal{L}_n^{TU-S}(\boldsymbol{A}) + \sum_{\alpha} \mathcal{L}_n^{TU-Eps}(\boldsymbol{A}) + \sum_{\alpha,Bausch.} \mathcal{L}_n^{Shear-S}(\boldsymbol{A}) + \mathcal{L}_n^{BT-S}(\boldsymbol{A})\end{aligned} \tag{26}$$

with N the number of tests in the database. Superscript 'TU-S' stands for the stress level in tension, 'TU-Eps' stands for the width strain in tension, 'Shear-S' stands for the stress level in shear and 'BT-S- stands for the stress level in balanced biaxial tension. The sum of α for tension and shear is performed over all orientations to RD and Bauschinger tests in simple shear are also taken into account (subscript 'Bausch.'). For each test, the gap between experiments and model is given by

$$\mathcal{L}_n(\boldsymbol{A}) = \frac{1}{M_n}\sum_{i=1}^{M_n} (\boldsymbol{Z}(\boldsymbol{A},t_i) - \boldsymbol{Z}^*(t_i))^T \mathcal{D}_n (\boldsymbol{Z}(\boldsymbol{A},t_i) - \boldsymbol{Z}^*(t_i)) \tag{27}$$

where M_n is the number of experimental points of the nth test, $\boldsymbol{Z}(\boldsymbol{A},t_i) - \boldsymbol{Z}^*(t_i)$ the gap between experimental $\boldsymbol{Z}^*$ and simulated output variables $\boldsymbol{Z}$ at time t_i, and $\mathcal{D}_n$ a weighting matrix for the nth test. The experimental database consists of tests with two observable variables, namely stress and strain components. A different weighting coefficient is affected for each of these observable variables, the value of which is chosen according to the uncertainty on the experimental measurements. For the shear stress, the value of the weighting coefficient is $\Delta\sigma_{XY} = 3$ MPa; for the uniaxial tensile tests, $\Delta\sigma_{XX} = 5$ MPa and $\Delta\varepsilon_{YY} = 0.002$ and for the balanced biaxial tensile test, $\Delta\sigma_{XX} = 5$ MPa. The database is made up of the uniaxial tensile tests at 0°, 45° and 90° to the RD for the DP500 and 0°, 22°, 45°, 77° and 90° to the RD for the DC04, taking into account the transverse strain, of the monotonic simple shear tests for the same orientations, of the three cyclic shear tests in the RD and of the balanced biaxial tensile test.

Although the viscous behavior has been observed in many metallic materials, the rate-independent constitutive models are still widely used to describe the mechanical behavior of sheets in quasi-static forming processes. The viscous behavior could be neglected by choosing suitable values of viscosity parameters, K_v and n_v, of Eq. (3) in an elasto-visco plastic constitutive model. In the present paper, the rate-independence is assumed, then the strain rate sensitivity parameters were fixed to $K_v = 5$ MPa s^{1/n_v} and $n_v = 4$, which leads to a viscous contribution of the order of 1.6 MPa at a strain rate of 10^{-3} s^{-1}. In order to check whether all the tests were performed within a similar strain rate range, the evolution of the equivalent viscoplastic strain is investigated in the simulations of uniaxial and balanced biaxial tension and shear in the RD as shown in Fig. 4. In uniaxial tension, the equivalent viscoplastic strain rate for these two steels is almost constant and of the same magnitude except for the sharp increase at the end of the test for DP500 since necking occurs. A similar evolution is observed in simple shear, but relates to different constant values. In addition, these rather constant strain rates in tension and simple shear leads to a constant overstress. On the contrary, a serious non-linearity of strain evolution with time is observed for the bulge test, which is caused by the rapid evolution of localization. From the minimum and maximum strain rates reached among these tests (DP500), the largest gap in the viscous contribution was estimated below 1 MPa which can be neglected when comparing it with the yield stress. Hence, the current fixed strain rate sensitivity parameters are reasonable to support the rate-independent assumption.

In general, the initial yield stress in tension and shear and plastic anisotropy coefficients are used to describe the initial anisotropy, and their evolution is related to the hardening behavior and strain-induced anisotropy. With the current identification strategy, the accurate prediction of anisotropy and hardening behavior is represented by a better description of flow stress in tension and shear and plastic anisotropy coefficients. It should be emphasized that in this work, plastic anisotropy coefficients are not directly used in the optimization procedure but the evolution of the transverse strain with respect to the longitudinal strain in tension. This data correspond to the raw data from experiments and r-values are simply calculated from it. In order to check the capability of the current identification strategy, three constitutive models are used to predict the anisotropy and hardening behavior of metallic sheets. The constitutive models are based on Hill's 1948 or Bron–Besson yield function, Swift isotropic hardening model and with or without Yoshida-Uemori kinematic hardening model, which are termed as 'Hill–Iso', 'Hill–Yoshida' and 'Bron–Yoshida', respectively.

Elastic properties were not optimized: Young's modulus is directly measured from tensile tests and values are 191 GPa for DP500 and 176 GPa for DC04. Poisson's ratio is fixed to 0.29 for both materials.

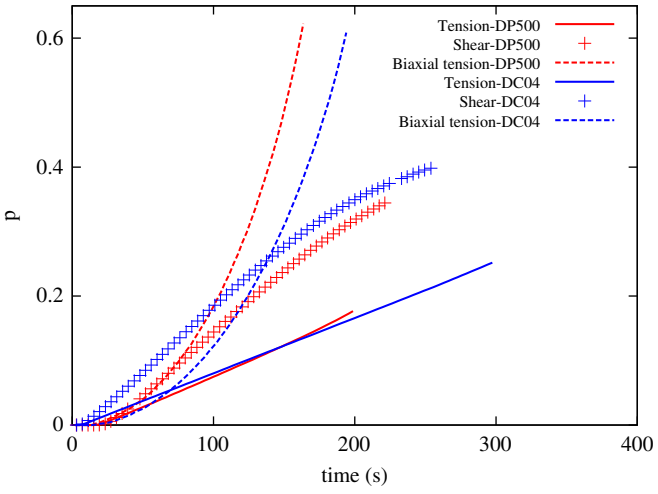

Fig. 4. Evolution of the equivalent viscoplastic strain p in uniaxial and balanced biaxial tension and simple shear at 0° to the RD, obtained with SiDoLo software. The material parameters used here correspond to the column termed as 'Bron–Yoshida' in Table 2.

4.2. Prediction of the anisotropy and hardening behavior for DP500

Material parameter identification for the three constitutive models is performed for the DP500 steel and values are listed in Table 2. With this set of parameters, the strain–stress responses in the uniaxial and balanced biaxial tension, monotonic and Bauschinger simple shear, and transverse strains in tension are predicted as shown in Figs. 5–7, as well as plastic anisotropy coefficients in Fig. 8.

The experimental and predicted Cauchy stress in uniaxial and balanced biaxial tensile, and monotonic simple shear tests at 0° to the RD are shown in Fig. 5(a). Concerning cyclic shear tests, the transient behavior, strain-hardening stagnation and permanent softening are experimentally observed in the Bauschinger simple shear tests (cf. Fig. 5(b)). Meanwhile, it is found that the strain-hardening stagnation increases with the prestrain. The flow stress of the balanced biaxial tensile test is larger than others, and presents more non-saturating hardening behavior. Hill–Yoshida and Bron–Yoshida constitutive models have almost the similar capability to predict the flow stress, however, the Cauchy stress predicted by Hill–Iso constitutive model is much lower at the end of the balanced biaxial tension, but higher under reversal simple shear since its incapability to predict the Bauschinger effect. It can be seen that Yoshida–Uemori model leads to an overall good description of the stress–strain curve after reloading in the opposite direction. However, the stagnation is too severe, indeed

Table 2
Material parameters for the DP500 and DC04 steel sheets; L and M for Hill's 1948 yield function and $c^k_{i\geq 5}$ for Bron–Besson yield function are irrelevant. The material parameters of Hill–Iso constitutive model are identified from the same material database except for the Bauschinger simple shear tests.

Model	Label	Unit	Hill–Iso		Hill–Yoshida		Bron–Yoshida	
			DP500	DC04	DP500	DC04	DP500	DC04
	F	–	0.488	0.282	0.492	0.289	–	–
Hill1948	G	–	0.461	0.264	0.459	0.267	–	–
yield function	N	–	1.589	1.754	1.607	1.807	–	–
	α	–	–	–	–	–	0.598	0.279
	a	–	–	–	–	–	2.008	1.141
	b^1	–	–	–	–	–	11.135	28.325
	b^2	–	–	–	–	–	8.216	2.869
	c^1_1	–	–	–	–	–	0.929	1.293
Bron–Besson	c^1_2	–	–	–	–	–	1.054	0.820
yield function	c^1_3	–	–	–	–	–	0.889	0.667
	c^1_4	–	–	–	–	–	0.962	0.718
	c^2_1	–	–	–	–	–	0.827	0.506
	c^2_2	–	–	–	–	–	0.639	0.776
	c^2_3	–	–	–	–	–	1.219	1.603
	c^2_4	–	–	–	–	–	0.970	1.327
	Y	MPa	259.3	135.2	196.7	129.9	188.7	145.2
	B	MPa	–	–	407.0	168.0	389.5	168.0
	C	–	–	–	248.7	657.9	246.3	637.4
Yoshida–Uemori	m	–	–	–	1.005	1.281	0.993	0.223
(or Isotropic)	b	MPa	–	–	196.2	8.980	181.991	25.242
hardening model	h	–	–	–	0.753	0.526	0.705	0.433
	K	MPa	832.9	567.1	731.1	558.6	704.2	601.8
	n	–	0.175	0.262	0.138	0.262	0.141	0.251

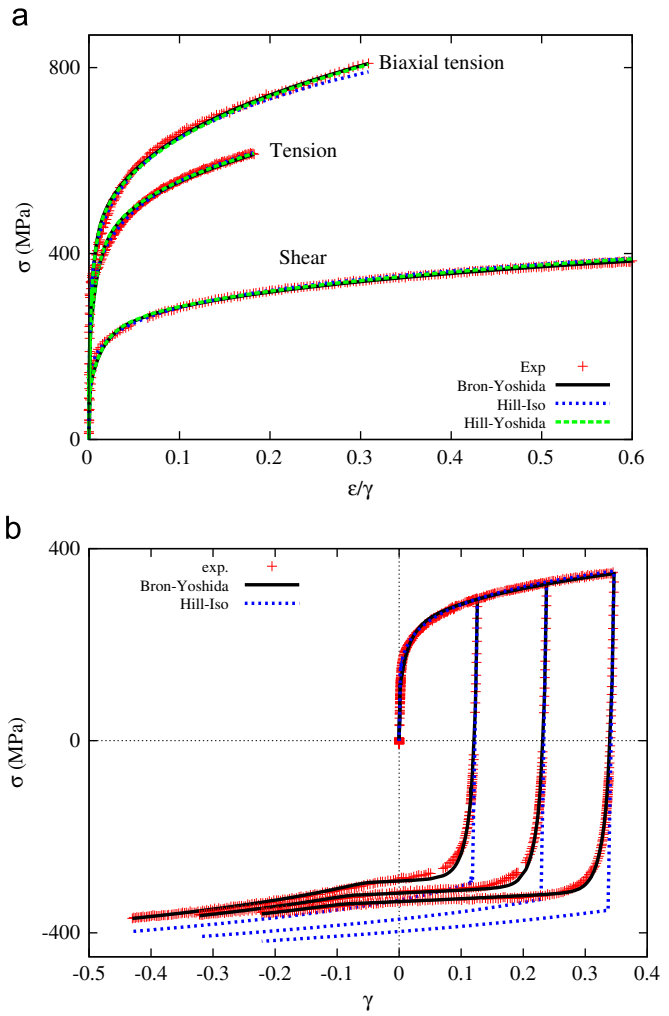

Fig. 5. Predicted Cauchy stress in uniaxial and balanced biaxial tensile tests and simple shear tests at 0° to the RD (DP500). ε stands for the logarithmic strain component ε_{XX} in tension and balanced biaxial tension, where $\vec{X}$ is parallel to the rolling direction. (a) Monotonic tests. (b) Cyclic shear tests.

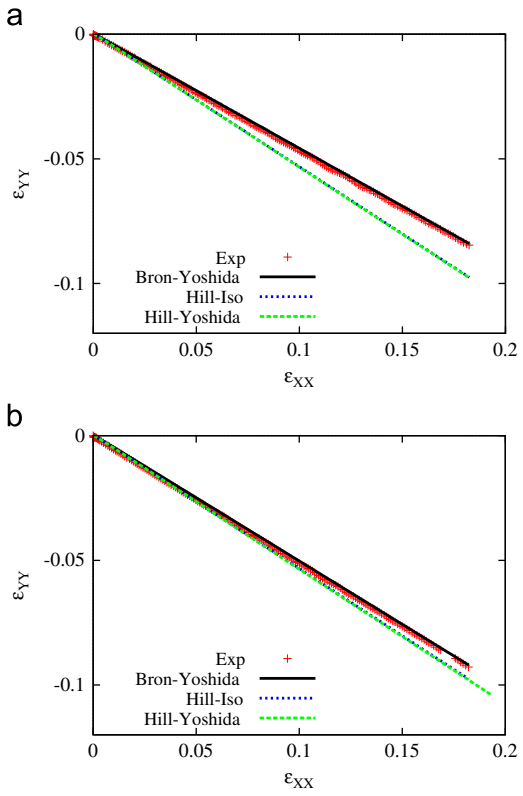

Fig. 6. Evolution of transverse strain with longitudinal strain in uniaxial tension (DP500). (a) 0°/RD. (b) 45°/RD.

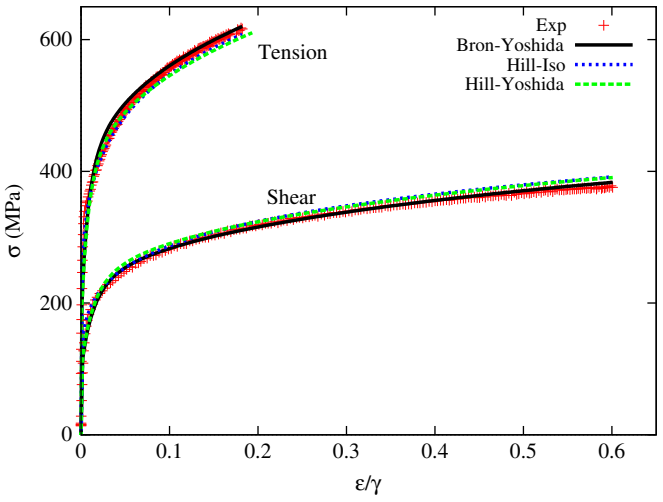

Fig. 7. Predicted Cauchy stress in uniaxial tensile tests and simple shear tests at 45° to the RD (DP500).

as can be seen from experiments in Fig. 5(b), the hardening rate decreases but remains positive whatever the prestrain. The simulated transverse strain ε_{YY} in uniaxial tension is compared in Fig. 6(a). It can be seen that ε_{YY} predicted by Hill–Iso or Hill–Yoshida constitutive model is similar and exhibits the largest gap with experiments, while ε_{YY} is better predicted by Bron–Yoshida model.

Fig. 7 shows that the gap between the Cauchy stress simulated by Hill–Iso or Hill–Yoshida constitutive model and experiments increases with plastic deformation in uniaxial tension at 45° to the RD, while the flow stress predicted by Bron–Yoshida fits well with experiments. In addition, the Cauchy stress calculated by Hill–Iso or Hill–Yoshida is lower than the experimental value. As for the simulated shear stress for these three models, the differences are rather small. The prediction of the transverse strain ε_{YY} in uniaxial tension at 45° to the RD is similar to that of tension in the RD as illustrated in Fig. 6(b). Similar results have been obtained at 90° to the RD and are not displayed here.

4.3. Prediction of the anisotropy and hardening behavior for DC04

In order to check the identification strategy for the more anisotropic material, the prediction of the anisotropy and hardening is also performed for the DC04 steel. Similarly to the DP500 steel, using material parameters in Table 2, the strain–stress responses in uniaxial and balanced biaxial tension, monotonic and Bauschinger simple shear, and transverse strains in tension are predicted as shown in Figs. 9–11, and plastic anisotropy coefficients are shown in Fig. 12.

The experimental and predicted Cauchy stress in uniaxial and balanced biaxial tensile, and monotonic and Bauschinger simple shear tests in the RD is shown in Fig. 9. The transient behavior, hardening stagnation and permanent softening are experimentally observed. Conversely to the DP500 steel, the flow stress of the balanced biaxial tensile test is much larger than that of uniaxial tension or simple shear. Similarly to the DP500 steel,

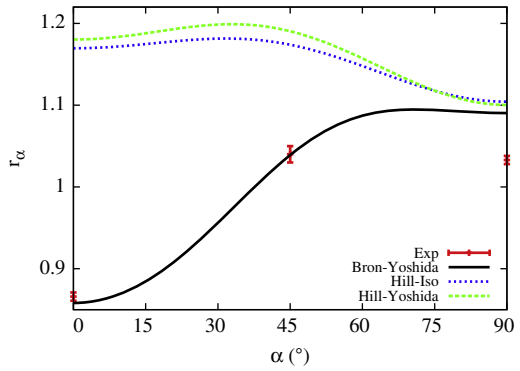

Fig. 8. Prediction of plastic anisotropy coefficients (DP500).

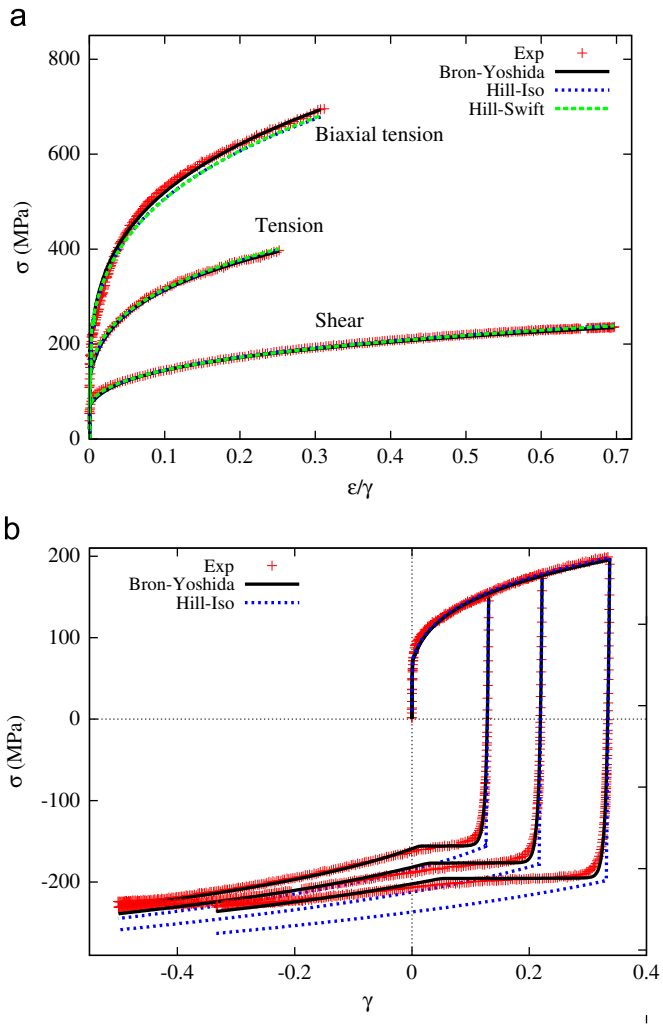

Fig. 9. Predicted Cauchy stress in uniaxial and balanced biaxial tensile tests and simple shear tests at 0° to the RD (DC04). ε stands for the logarithmic strain component ε_{XX} in tension and balanced biaxial tension, where $\vec{X}$ is parallel to the rolling direction. (a) Monotonic tests. (b) Cyclic shear tests.

the Cauchy stress predicted by Hill–Iso constitutive model is slightly lower than others at the end of balanced biaxial tension. The transverse strain ε_{YY} predicted by Hill–Iso or Hill–Yoshida constitutive model is the same and also exhibits the largest gap with experiments, while ε_{YY} predicted by Bron–Yoshida model is much closer to the experiments, as compared in Fig. 10(a).

Fig. 11 shows that these three constitutive models have almost the similar capability to predict flow stress in uniaxial tension

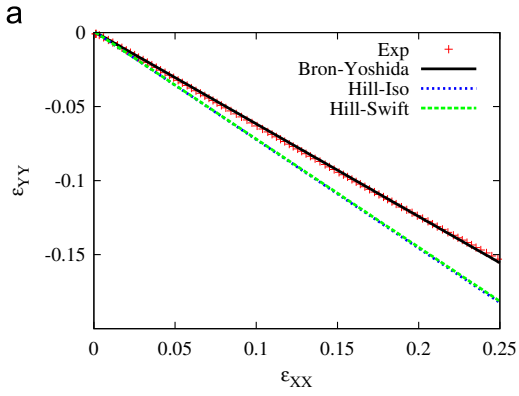

Fig. 10. Evolution of transverse strain with longitudinal strain in uniaxial tension (DC04). (a) 0°/RD. (b) 45°/RD.

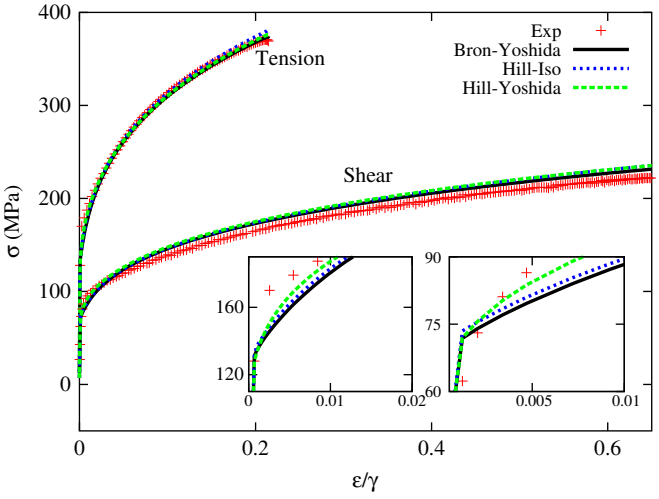

Fig. 11. Predicted Cauchy stress in uniaxial tensile tests and simple shear tests at 45° to the RD (DC04).

and simple shear at 45° to the RD. However, the flow stress predicted by Bron–Yoshida model fits better with experiments. Still, it can be noted that all these constitutive models cannot well predict the initial yield stress, i.e. the current identification strategy loses some accuracy on the description of the initial yield for the more anisotropic material. As for the prediction of transverse strain ε_{YY} in uniaxial tension, a good description is obtained with Bron–Yoshida constitutive model as shown in Fig. 10(b). The prediction of the stress and transverse strain ε_{YY} in uniaxial tension at the other directions to the RD is similar to those at 0° and 45°.

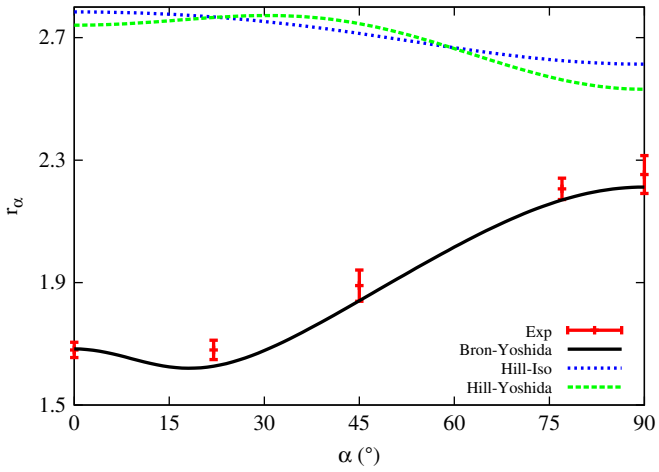

Fig. 12. Prediction of plastic anisotropy coefficients (DC04).

4.4. Discussion

For both materials, Hill's 1948 yield function has a poor capability to model transverse strain since it lacks degrees of freedom and since the weight was put on stress level, in order to correctly predict the Bauschinger effect. Indeed, from Eq. (19), it comes that only three material parameters are independent in the plane stress condition. While seven stress states and three transverse strains for the DP500 steel, and 11 stress states and five transverse strains for the DC04 steel, are used to identify the material parameters of the constitutive models. Thus, serious over-constraints should exist in the determination of the material parameters of Hill's 1948 yield function. To achieve the overall compromise of the prediction over all the tests, a poor description is reached for each test.

On the contrary, Bron–Besson yield function, with 12 independent parameters in case of plane stress state is expected to accurately predict both the anisotropy and hardening behavior of metallic sheets. However, one large error point is observed in the prediction of the anisotropy coefficient for the DP500 steel as illustrated in Fig. 8, although Bron–Yoshida constitutive model describes accurately the flow stress. This is mainly caused by the measure of the plastic anisotropy coefficient. Usually, this coefficient is measured in a given strain range. With this method, the experimental plastic anisotropy coefficient is significantly influenced by the choice of the strain range. In this condition, the experimental coefficient cannot correctly describes the transverse strain in tension. In addition, the distribution of experimental points of ε_{YY} for the DC04 steel is uniform with a constant sampling frequency, which is different with that of the DP500 steel. It indicates that the measured anisotropy coefficient for the DC04 steel can accurately express the transverse strain ε_{YY} since no necking occurs, as illustrated in Fig. 12.

Considering results obtained both with Hill48–Iso and Hill48–Yoshida models, it can be seen that the predicted plastic anisotropy coefficients are similar, though rather far from experimental results. This similarity comes from the fact that the evolution law of $\boldsymbol{X}$, which brings the largest contribution to the kinematic part of hardening, is written according to [14].

The main point for using Yoshida–Uemori model is to predict the work-hardening stagnation recorded after a Bauschinger test [15]. This stagnation has been evidenced both with tension-compression tests [16] and cyclic simple shear tests. This last strain path is particularly well suited for strain path reversal, in the sense that it allows an equivalent plastic prestrain up to 0.2 to be investigated and to reach after straining an equivalent plastic strain of 0.5. In order to highlight this stagnation, the work-hardening rate $d\sigma/d\gamma$ has been calculated by fitting splines on the stress–strain curves of Fig. 9(b), considering both the experiments and the simulation, and by finite difference derivation. Fig. 13 shows that the experimental work-hardening rate remains strictly positive whatever the prestrain value, which is consistent with previously published results [15]. Therefore, though the magnitude of the plateau is well represented, the hardening rate predicted by Yoshida–Uemori is too small compared to the experiments. The prediction of the mechanical behavior in reloading after a prestrain could be further improved by modifying the parameter C, as suggested in [17].

The current identification strategy focuses simultaneously on both the initial and strain-induced anisotropy, thus avoiding to get the initial yield stress and plastic anisotropy coefficients. Hence, better prediction on transverse strain in tension and flow stress in uniaxial and balanced biaxial tension and simple shear is achieved.

Among the three constitutive models, Bron–Yoshida constitutive model accurately predicts both the flow stress and transverse strain ε_{YY} for all the tests as expected, although the current identification strategy loses some accuracy in the prediction of the initial yield stress. The comparison of the final values of the cost function is shown in Fig. 14. The cost function is an indicator of the gap between experimental and simulated values. It depends also on the number of tests in the experimental database and on the weighting coefficients. In this work, the experimental database is the same for all simulations and the weighting coefficients are kept constant. Comparing with Hill–Yoshida constitutive model, the reduction of the cost function with Bron–Yoshida model is very clear, it is around 7% for DP500 steel and 45% for DC04 steel.

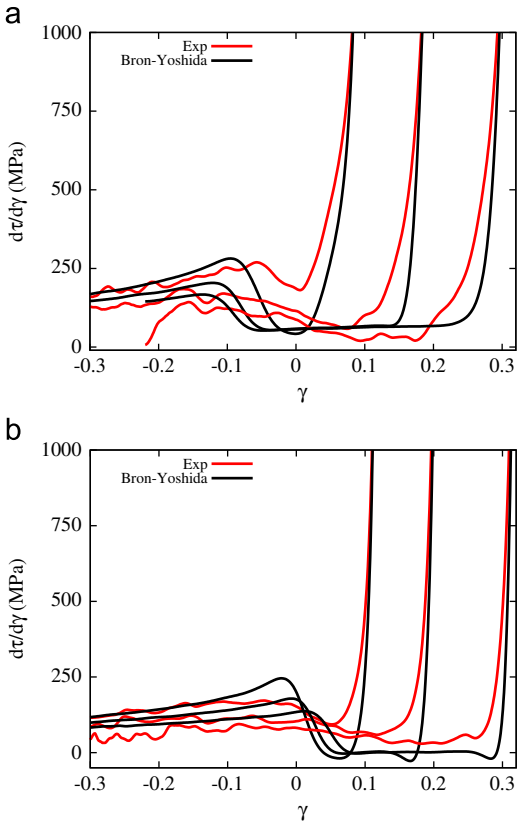

Fig. 13. Work-hardening rate, calculated as $d\tau/d\gamma$ evolution versus shear strain during cyclic shear tests. Only the reversed loading path is plotted. (a) DP500. (b) DC04.

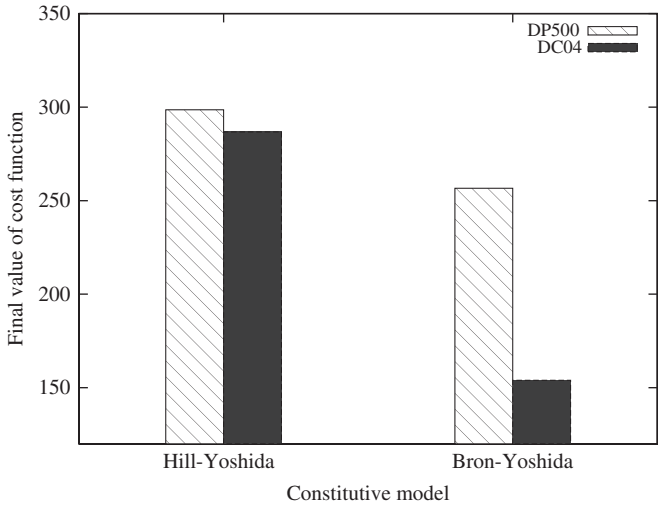

Fig. 14. Comparison of the final values of cost function with different constitutive models.

5. Conclusion

In this paper, characterization of the anisotropy and hardening behavior of DP500 and DC04 steels is presented as well as their modeling within an elasto-viscoplasticity framework, based on Bron–Besson yield function [5] and Yoshida–Uemori kinematic hardening model [6]. Tests in uniaxial tension, monotonic and Bauschinger simple shear and balanced biaxial tension are considered. The anisotropy and hardening behavior are identified from the stress–strain curves and transverse strain in tension, to consider the subsequent evolution of the plasticity surface after the initial yield. It is shown that this identification strategy loses some accuracy on the description of the initial yield stresses, but gains more accuracy in the prediction of the global hardening behavior. Hill's 1948 yield function is also chosen for comparison's sake. The results show that Bron–Besson yield function can well describe the anisotropy of the yield stress and transverse strain in uniaxial tension at the same time, whereas Hill's 1948 yield function only works for one of them. It indicates that such advanced anisotropic yield function should be used in the prediction of the anisotropy when more than tension is expected to be accurately reproduced, even for the steel with a nearly isotropic mechanical behavior.

Acknowledgments

The authors would like to thank the Région Bretagne and Direction Générale des Entreprises for their financial support.

References

[1] Yoshida F, Uemori T, Fujiwara K. Int J Plast 2002;18:633–59.
[2] Boger RK, Wagoner RH, Barlat F, Lee MG, Chung K. Int J Plast 2005;21: 2319–43.
[3] Rauch EF. Mater Sci and Eng A 1998;241:179–83.
[4] Flores P, Duchene L, Bouffioux C, Lelotte T, Henrard C, Pernin N, VanBael A, He S, Duflou J, Habraken AM. Int J Plast 2007;23:420–49.
[5] Bron F, Besson J. Int J Plast 2004;20:937–63.
[6] Yoshida F, Uemori T. Int J Mech Sci 2003;45:1687–702.
[7] Dunne F, Petrinic N. Introduction to computational plasticity. 2nd ed. New York: Oxford University Press; 2006.
[8] Thuillier S, Manach PY. Int J Plast 2009;25:733–51.
[9] Chaboche JL. Int J Plast 2008;24:1642–93.
[10] Dafalias YF, Popov EP. J Appl Mech 1976;98:645–51.
[11] Yoshida F, Uemori T, Abe S, Hino R. In: Proceedings of numisheet. Interlaken, Switzerland; 2008. p. 19–24.
[12] Hill R. Proc R Soc London 1948;193:281–97.
[13] Chaparro BM, Thuillier S, Menezes LF, Manach PY, Fernandes JV. Comput Mater Sci 2008;44:339–46.
[14] Ziegler H. Q Appl Math 1959;17:55–65.
[15] Hu Z. Acta Metall Mater 1994;42:3481–91.
[16] Cao J, Lee W, Cheng HS, Seniw M, Wang HP, Chung K. Int J Plast 2009;25:942–72.
[17] Yoshida F, Uemorim T. Int J Plast 2002;18:661–86.